

On the Coherence of WMAP and Planck Temperature Maps

András Kovács^{1,2}, Julien Carron³ and István Szapudi³

¹ *Institute of Physics, Eötvös Loránd University, 1117 Pázmány Péter sétány 1/A Budapest, Hungary*

² *MTA-ELTE EIRSA “Lendulet” Astrophysics Research Group*

³ *Institute for Astronomy, University of Hawaii 2680 Woodlawn Drive, Honolulu, HI, 96822, USA*

Submitted 2013

ABSTRACT

The recent data release of ESA’s Planck mission together with earlier WMAP releases provide the first opportunity to compare high resolution full sky Cosmic Microwave Background temperature anisotropy maps. To quantify the coherence of these maps beyond the power spectrum we introduce Generalized Phases, unit vectors in the $2\ell + 1$ dimensional representation spaces. For a Gaussian distribution, Generalized Phases are random and if there is non-Gaussianity, they represent most of the non-Gaussian information. The alignment of these unit vectors from two maps can be characterized by their angle, 0° expected for full coherence, and 90° for random vectors. We analyze maps from both missions with the same mask and $N_{side} = 512$ resolution, and compare both power spectra and Generalized Phases. We find excellent agreement of the Generalize Phases of Planck Smica map with that of the WMAP Q,V,W maps, rejecting the null hypothesis of no correlations at 5σ for ℓ ’s $\ell < 700$, $\ell < 900$ and $\ell < 1100$, respectively, except perhaps for $\ell < 10$. Using foreground reduced maps for WMAP increases the phase coherence. The observed coherence angles can be explained with a simple assumption of Gaussianity and a WMAP noise model neglecting Planck noise, except for low-intermediate ℓ ’s there is a slight, but significant off-set, depending on WMAP band. On the same scales WMAP power spectrum is about 2.6% higher at a very high significance, while at higher ℓ ’s there appears to be no significant bias. Using our theoretical tools, we predict the phase alignment of Planck with a hypothetical perfect noiseless CMB experiment, finding decoherence at $\ell \simeq 2900$; below this value Planck can be used most efficiently to constrain non-Gaussianity.

Key words: cosmology: observations – cosmology: theory – cosmic background radiation

1 INTRODUCTION

One of the principal goals of modern cosmology is to characterize the statistical properties of the primordial density fluctuations, i.e. the seeds of the present large-scale structure. As widely presumed, the initial perturbations are associated with quantum properties of an inflationary field (Guth 1981). If this model is correct, the primordial fluctuations should be overwhelmingly Gaussian (Bardeen et al. 1986; Bond & Efstathiou 1987) along with the small temperature fluctuations of the Cosmic Microwave Background (CMB) sky.

Gaussianity is the most fundamental prediction of inflation. Randomness of the complex phases of the harmonic coefficients of small CMB temperature fluctuations provides natural constraints, since departures from Gaussian behavior typically cause deviations from randomness (Coles & Chiang 2000). There are several methods constraining non-Gaussianity from phase information: phase mapping and uniformity tests (Chiang et al. 2002, 2004), Shannon entropy of phases (Chiang & Coles 2000), surrogates (Raeth et al. 2010), random walks (Stannard & Coles 2005; Hansen et al. 2011), etc. These have been applied to WMAP all-sky maps, and most re-

cently to Planck (Planck Collaboration et al. 2013c). In some cases, non-Gaussian residuals have been detected (Chiang et al. 2003; Naselsky et al. 2005), although no primordial non-Gaussianity has been found with any certainty.

Other studies, such as Land & Magueijo (2005a,b, 2007); Copi et al. (2004, 2006) and Bielewicz et al. (2005) defined directions on a sphere at each ℓ to construct estimators constraining unusual alignments and correlations in the harmonic series representing the CMB maps. Several “anomalies” and alignments were identified, and several tests have been performed to explore their origin (Francis & Peacock 2010; Frommert & Enßlin 2010; Rassat et al. 2013). These marginally significant anomalies were originally detected in WMAP, and recently confirmed in Planck (Planck Collaboration et al. 2013c).

In this work we generalize methods based on complex phases by introducing Generalized Phases (hereafter GPs), unit vectors in $(2\ell + 1)$ dimensional representation spaces. GPs relate to the $SO(3)$ group as complex phases to the $U(1)$ group, in particular, they correspond to a random direction for a Gaussian field. They represent most of the information beyond the measured power spectrum, and for a Gaussian distribution they are independent from it. Neverthe-

less, two observations of the same CMB realization should have exactly the same phases. The principal aim of this work is to use this simple property to construct a rigorous and concise ℓ -by- ℓ comparison of WMAP and Planck maps that emphasizes information beyond the power spectrum. In particular, we will characterize coherence of two maps by the angle of the unit vectors corresponding to their GPs, that also corresponds to a correlation coefficient in harmonic space.

We organize this paper as follows. In Section 2 we describe the data we used, and introduce our methods including theoretical expectations, simulations and measurements. In Section 3 our results, and statistical significances of our findings are presented. Finally, we briefly summarize our results in Section 4. The appendix contains derivations of formulae used in the main text.

2 DATA AND METHODS

To quantify the coherence of WMAP and Planck we first prepare maps of the same resolution. The WMAP team provides $N_{side} = 512$ CMB temperature maps, therefore we choose this as our base resolution. The Planck CMB products have higher resolution, $N_{side} = 2048$, thus we downgraded Planck maps using HEALPIX (Gorski et al. 2005) for $N_{side} = 512$. We also used the $N_{side} = 512$ WMAP9 Temperature Analysis Mask that leaves 78% of the sky for our analysis.

For WMAP, we used the Q,V,W frequency bands downloaded from the LAMBDA website ¹, using both original and foreground reduced versions. (Jarosik et al. 2011; Bennett et al. 2012). For Planck, we downloaded the NILC and Smica CMB maps (Planck Collaboration et al. 2013b) from the Planck Legacy Archive ². They already have galactic foregrounds and known point sources removed.

2.1 Generalized Phases

The CMB temperature fluctuations can be expanded into spherical harmonics:

$$\frac{\Delta T}{T}(\vartheta, \varphi) = \sum_{\ell=0}^{\infty} \sum_{m=-\ell}^{\ell} a_{\ell m} Y_{\ell m}(\vartheta, \varphi) \quad (1)$$

Phases are defined by complex $a_{\ell m}$ coefficients of CMB multipoles as follows

$$a_{\ell m} = |a_{\ell m}| \cdot \exp(i\phi_{\ell m}) \quad (2)$$

These Fourier phases generate rotations around the z -axis, corresponding to to the U(1) subgroup of the full SO(3) symmetry of the harmonic coefficients. For Gaussian random fields (GRF), Fourier phases are random and uniformly distributed between 0 and 2π . Testing the randomness of these phases therefore provides an interesting diagnostic of the Gaussianity of the fluctuation field (Coles & Chiang 2000). Note that the power at each ℓ and these phases do not fully determine the random field.

To generalize complex Fourier phases, we first build $(2\ell + 1)$ dimensional vectors using real and imaginary parts of $a_{\ell m}$ coefficients:

$$\varepsilon_{\ell} = (a_{\ell 0}/\sqrt{2}, \text{Re}[a_{\ell 1}], \dots, \text{Re}[a_{\ell \ell}], \text{Im}[a_{\ell 1}], \dots, \text{Im}[a_{\ell \ell}]) \quad (3)$$

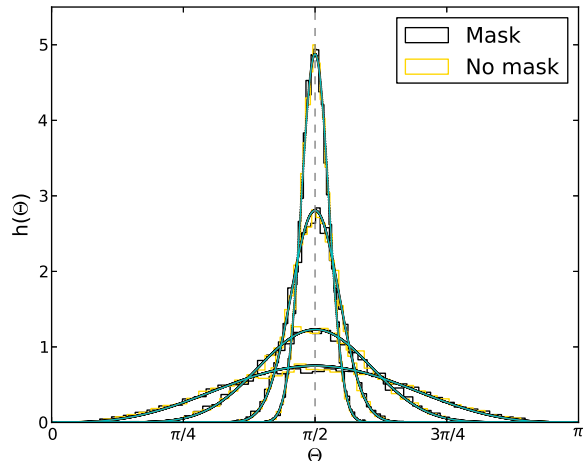


Figure 1. Distributions of angles between random unit vectors in $(2\ell + 1)$ dimensions. We compare analytic expectations and simulations, and test properties of galactic masks, as well. We present $\ell = 2, 5, 25, 75$ cases. These illustrate that angles are concentrated around $\pi/2$. This concentration becomes stronger as the dimension n grows. These results are insensitive to the galactic mask as long as the unit vectors are truly random.

These vectors contain all the information due to the reality of the underlying random field. For a Gaussian field, this is a random vector, with each elements of ε_{ℓ} having a variance of $C_{\ell}/2$. Generalized Phases are now defined as $(2\ell + 1)$ dimensional unit vectors

$$\hat{\varepsilon}_{\ell} = \frac{\varepsilon_{\ell}}{\sqrt{\sum_k \varepsilon_{\ell, k}^2}}. \quad (4)$$

For a Gaussian distribution, the GPs are uncorrelated, and for each ℓ they follow uniform distributions over the sphere $S^{2\ell}$. The statistics of GPs contain information complementary to the power spectrum, and for mildly non-Gaussian distributions, they should contain most of the non-Gaussian information. If the power and the GPs are given, the realization of a random field is fully constrained.

In this work, we compare Generalized Phases to quantify the (generalized) phase coherence of WMAP and Planck maps, i.e. the ℓ -by- ℓ coherence of the maps beyond and independently of the match of their power spectra. Next we present some basic results on the statistics of these phases.

2.2 Random angle statistics in n dimensions

Angles between Generalized Phases of two uncorrelated datasets - e.g. CMB realizations - should be random, their distributions are characterized by analytic formulae (Cai et al. 2013). When the dimension $n = 2\ell + 1$ is fixed, the distribution of angles has a density function given by

$$h(\Theta) = \frac{1}{\sqrt{\pi}} \frac{\Gamma(\frac{n}{2})}{\Gamma(\frac{n-1}{2})} \cdot \sin^{n-2} \Theta. \quad (5)$$

Note that if $n = 2$, $h(\Theta)$ is the uniform density on $[0, \pi]$. When $n \geq 3$, $h(\Theta)$ is a unimodal distribution with peak position of $\Theta = \pi/2$. The concentration around $\pi/2$ becomes stronger as n grows, since $\sin^{n-2} \Theta$ is driven to zero quickly for $\Theta \neq \pi/2$ (Cai et al. 2013). This means that uncorrelated vectors in high dimensions tend to be perpendicular. As expected, in large dimensions, the distribution

¹ <http://lambda.gsfc.nasa.gov/>

² <http://www.sciops.esa.int/index.php?project=PLANCK>

tends to a Gaussian distribution centered on $\pi/2$. In Fig. 1 we show estimates of distributions of random angles in higher dimensions. We simulated 500 CMB skies to test Eq. (5). Simulations were made by using WMAP9 cosmological parameters, and WMAP9 noise. We randomly choose 10,000 pairs of CMB simulations, and calculate Generalized Phases. Four examples of $\ell = 2, 5, 25, 75$ illustrate that individual distributions of angles between random unit vectors in $(2\ell + 1)$ dimensions follow Eq. (5) closely. We checked that these results hold up to $\ell = 1535$, the maximum we can measure with our maps.

We repeated our measurements on masked CMB skies using WMAP9 Temperature Analysis Mask. According to Fig. 1, and perhaps somewhat surprisingly, no difference was found. While galactic mask strongly affects statistical analysis of normal phases (Chiang & Naselsky 2007), the distribution of Θ is insensitive to the mask.

It is useful to consider the closely related correlation coefficient $\cos \Theta = C_\ell^{AB} / \sqrt{C_\ell^A C_\ell^B}$ in addition to Θ . In this case, $x = (\cos \Theta + 1)/2$ follows the Beta distribution on $[0, 1]$, i.e. $x^{\alpha-1}(1-x)^{\beta-1}/B(\alpha, \beta)$ with parameters $\alpha = \beta = (n-1)/2 = \ell$. Thus the exact first two moments of $\cos \Theta$ are

$$\langle \cos \Theta \rangle = 0, \quad \langle \cos^2 \Theta \rangle = \frac{1}{n} \quad (6)$$

2.3 CMB and noise

WMAP and Planck measurements of the CMB sky contain noise. This noise induces a rotation of the unit vectors $\hat{\epsilon}_\ell^{\text{CMB}}$ on the 2ℓ dimensional sphere. Assuming full sky coverage and isotropic Gaussian noise, these rotations will only depend on the respective spectra of the CMB and that of the noise. The angles obey

$$\cos \Theta_\ell = \frac{\epsilon_\ell^{\text{CMB}} \cdot (\epsilon_\ell^{\text{CMB}} + \epsilon_\ell^{\text{noise}})}{|\epsilon_\ell^{\text{CMB}}| |\epsilon_\ell^{\text{CMB}} + \epsilon_\ell^{\text{noise}}|}. \quad (7)$$

In the case of Gaussian noise, it is possible to obtain an explicit form for the distribution of the angle, generalizing (5). Introducing the signal to noise SN as the ratio of the norms of the two vectors,

$$SN = \frac{|\epsilon_\ell^{\text{CMB}}|}{|\epsilon_\ell^{\text{noise}}|} = \sqrt{\frac{C_\ell^{\text{CMB}}}{C_\ell^{\text{noise}}}}, \quad (8)$$

one finds (see Appendix A for details)

$$h_N(\Theta) = \frac{\Gamma(n)}{\Gamma(\frac{n-1}{2})} \sin^{n-2} \Theta \cdot \exp\left(-\frac{n}{2} SN^2 \sin^2 \Theta\right) i^{n-1} \text{erfc}\left(-\sqrt{\frac{n}{2}} SN \cos \Theta\right), \quad (9)$$

where the special functions

$$i^n \text{erfc}(z) = \frac{2}{\sqrt{\pi}} \int_z^\infty dt \frac{(t-z)^n}{n!} e^{-t^2} \quad (10)$$

are the iterated integrals of the complementary error function (Abramowitz & Stegun 1970). These functions satisfy convenient recursion relations allowing easy generation of $h_N(\Theta)$. With the help of $i^n \text{erfc}(0) = 2^{-n}/\Gamma(n/2 + 1)$ we can check that we recover the corresponding distribution (5) for Θ in the limit of vanishing signal to noise, as expected.

Again, the density function is very close to a Gaussian. Useful simple approximations for its mean and variance are

$$\langle \cos \Theta \rangle \approx \frac{SN}{\sqrt{1+SN^2}} = \sqrt{\frac{C_\ell^{\text{CMB}}}{C_\ell^{\text{CMB}} + C_\ell^{\text{noise}}}} \quad (11)$$

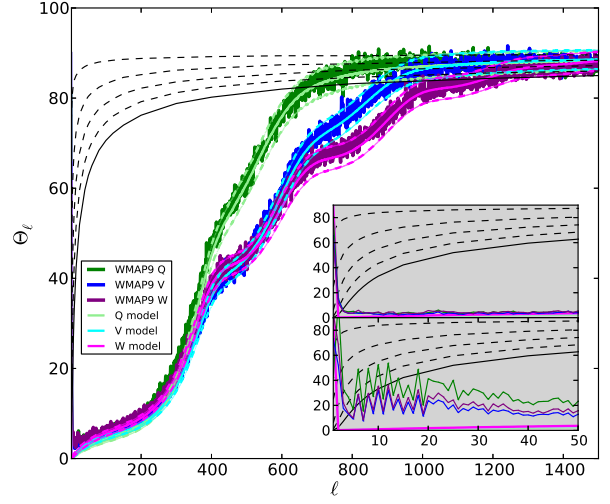


Figure 2. The measured and theoretically predicted angles between Generalized Phases of Planck Smica map, and WMAP products. A black solid line defines the 5σ alignment confidence level, while dashed black curves correspond to 4σ , 3σ , 2σ , and 1σ values. The top inset zooms on $\ell < 50$, while bottom inset shows the same without foreground cleaning.

and

$$\langle \cos^2 \Theta \rangle - \langle \cos \Theta \rangle^2 \approx \frac{1}{n} \frac{1 + SN^2/2}{(1 + SN^2)^3}. \quad (12)$$

Both of these approximations are already at least 5% accurate for any value of SN at $\ell = 5$.

3 RESULTS

We obtained Generalized Phases of WMAP and Planck datasets by applying Equations (3) and (4). We present our results for the Planck Smica map, but repeating all our analysis with the NILC map produced virtually identical results. To quantify the coherence of the two maps, we calculated dot products of unit vectors defined by individual datasets at each ℓ multipole as

$$\cos \Theta_\ell = \sum_k \hat{\epsilon}_{\ell,k}^{\text{Planck}} \cdot \hat{\epsilon}_{\ell,k}^{\text{WMAP}}. \quad (13)$$

We choose the above angle to characterize the coherence of the maps. While this angle does not contain all information, indeed there are many ways of constructing a unit vector that is at angle Θ with respect to another one, it corresponds to a concise way of expressing coherence, and we can additionally interpret $\cos \Theta_\ell$ in terms of C_ℓ 's as a correlation coefficient $C_\ell^{\text{WMAP,Planck}} / \sqrt{C_\ell^{\text{WMAP}} C_\ell^{\text{Planck}}}$, i.e. 60° means 50% correlation between the two maps.

To quantify the coherence, we choose as our null hypothesis that the two maps are *not* correlated. In that case the distribution Θ_ℓ follows analytic distributions of Eq. (5), and p -values can be calculated by integrating Eq. (5) to the measured Θ_ℓ . We define the two maps as significantly correlated if the null hypothesis can be rejected at the 5σ level.

Figure 2 shows our results, where we compare Planck Smica map to WMAP Q, V and W band measurements. In general, the

correlation between the maps decreases with ℓ , as qualitatively expected in the presence of uncorrelated noise. For the lowest ℓ 's the null hypothesis cannot be rejected at the 5σ level, especially for the Q band, but using foreground reduced maps improves the correlation to the point that maybe only the dipole is incoherent. This, however, only reflects the different cleaning procedures used by WMAP and Planck. In particular, the Smica algorithm sets $\ell = 0, 1$ exactly to zero, therefore it contains no information on the CMB (Jean-Francois Cardoso, private communication). The pattern illustrated on Figure 3 was also detected by Frejsel et al. (2013).

For higher ℓ 's, the monotonically increasing p -values reach the limit confidence levels corresponding to 5σ . We define these ℓ 's corresponding to decoherence at $\ell \approx 700$, $\ell \approx 900$ and $\ell \approx 1100$ for Q, V and W maps, respectively. This result is robust whether we use foreground removed WMAP maps or not, or Planck Smica/NILC maps. The observed decoherence can be fully explained based on a WMAP noise model, as illustrated in our Figure 2, and explained in more detail next. Our interpretation is that WMAP GPs are dominated by noise above these ℓ 's.

Our theory of Eq. 9 using simple Gaussian assumption for both the CMB and noise provides a prediction for the expected coherence angle between the maps. The agreement is excellent with both simulations and measurements at all ℓ 's, although there appears to be small but significant bias in the measurements at low-intermediate ℓ 's. Figure 4 displays the residual Θ_ℓ , i.e. the difference between our theoretical predictions for the decoherence based on our noise model, and the measured angle. For each Q,V and W, there appears to be an excess angle, i.e. more decoherence than predicted, for $\ell \lesssim 500, 400$ and 300 , respectively.

At face value in the framework of our simple assumptions, this would be a sign of excess noise not taken into account in our noise model. It needs to be emphasized though that this is a small, (although) significant effect, and therefore should be interpreted cautiously, given the assumption of uncorrelated Gaussian noise; noise correlations, foregrounds, and/or leakage from the dipole (e.g. Prunet et al. (2005); Das & Souradeep (2013)) could all influence the coherence angle in subtle ways.

For completeness, we measured power spectrum of the Planck Smica map, cross-power spectra of WMAP9 Q1-Q2, V1-V2, and an average cross-spectrum of six combinations of W1-W4 differential assemblies with SpICE (Szapudi et al. 2001): the power spectrum is complementary to the GPs, corresponds to the amplitude of the vector we defined in Eq. 3, and might give additional insight into the decoherence at low-intermediate ℓ 's. We used WMAP9 beam transfer function products for Q1, Q2, V1, V2, W1, W2, W3, and W4 maps, and a 5' Gaussian smoothing for the Smica map. We emphasize that we used again the same resolution maps, with the same mask, and the same method to measure the power spectrum for all maps, thus our comparison is more immediate than taking final products from the WMAP and Planck team, respectively.

The power spectra are consistent with each other for the most part, but curiously, in approximately the same range of ℓ 's, where we found less coherence than predicted by our theory, we find that $\tilde{C}_\ell^{\text{WMAP}}$ is on average 2.6% higher than $\tilde{C}_\ell^{\text{Planck}}$ in the three Q,V,W maps. For the sake of consistency, we consider multipoles between 10 and 300 for each band, and find that the WMAP spectra are 2.7%, 2.6% and 2.5% higher than Smica, respectively. While visual inspection confirms the significance of this bias, we estimated it quantitatively in Appendix B to be in the range of 10's of σ 's. This bias is confined to these scales, the inclusion of higher multipoles result in a non-detection of significant bias. While it would be difficult to assess quantitatively whether the bias persists

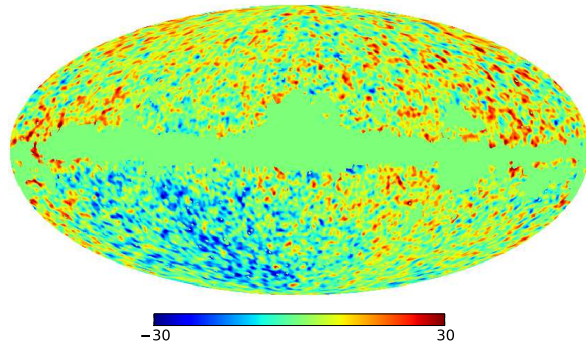


Figure 3. Difference map of Planck Smica and WMAP9 Internal Linear Combination (ILC) maps in μK , smoothed at 2 deg. See text for details.

on larger ℓ 's, at least qualitatively, it appears from Figure 4 that the bias is not significant above the the same $\ell \gtrsim 500, 400$ and 300 for Q,V, and W, respectively, where our theory predicts the decoherence based on the simple Gaussian WMAP noise model. This might be a tantalizing hint, but more investigations are needed to establish whether the two small, but significant effects are related.

We repeated our measurements with WMAP 7 year foreground cleaned data, and found similar trends in terms of Θ_ℓ angles. The agreement with WMAP9 results is less accurate, when we analyze maps without cleaning of foregrounds, but the difference is only significant at low ℓ 's. The most important observation, however, is that the estimated 5σ decoherence is at slightly lower ℓ if we use WMAP 7 year products. This is consistent with WMAP7 having more noise than WMAP9 further supporting the thesis that all experiments observe the same underlying CMB, and that instrumental noise causes the observed decoherence.

3.1 Decoherence from WMAP noise and impact of mask at high ℓ

So far we established that the decoherence observed on Figure 2 is expected to originate primarily from the noise in WMAP. Assuming that the level of noise in the Smica map is negligible with respect to that of the Q,V,W maps on these scales, we can test this hypothesis using our density functions in Eq. (9). We proceeded as follows. Assuming white noise σ_N^2 in each WMAP maps, the signal to noise is $SN = C_\ell^{\text{CMB}}/\sigma_N^2$, where C_ℓ^{CMB} was generated with the CAMB package³ with Planck's best fit parameters (Planck Collaboration et al. 2013a), multiplied by the respective beam window function of the Q,V or W maps. The solid lines in Figure 2 show the mean of the density function, and the dashed ones correspond to 2σ deviations. The decoherence is in excellent quantitative agreement with this simple model. It makes no difference to use the exact $h_N(\Theta)$ in Eq. (9) or the approximations in Eqs. (11) and (12).

The noise dominates by orders of magnitude at the highest ℓ 's, therefore an angle of 90 degrees is expected naively. The observed angles, however, deviate slightly from this theoretical prejudice, indicating a few percent residual correlation. As we show in more detail in Appendix C, this correlation is due to leakage of low ℓ power into higher ℓ 's, and essentially white noise. We can obtain accurate

³ <http://camb.info/>

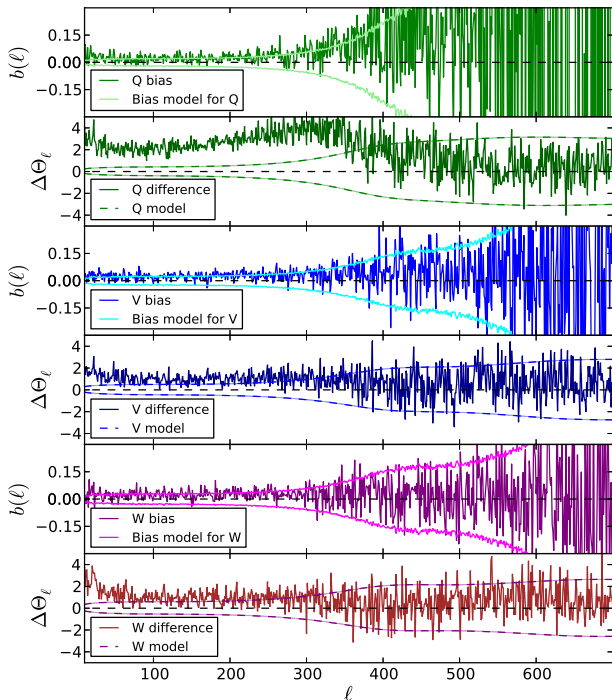


Figure 4. We show measured biases of power spectra for Q, V and W bands, while estimated 2σ deviations are shown by solid lines. In addition, discrepancies between modeled and measured Θ_ℓ are illustrated for Q, V and W, where dashed lines correspond to 2σ differences in our model.

analytic approximations assuming an azimuthally symmetric mask centered on the equator and white noise. The mask is an equatorial band sustaining an angle b with the equator, so that $f_{\text{sky}} = 1 - \sin b$. Using the explicit formula relating the spectrum \tilde{C}_ℓ of the masked field to that of the unmasked field C_ℓ (Hivon et al. 2002), we derive in Appendix C the asymptotic behavior of the spectrum,

$$\tilde{C}_\ell \rightarrow \frac{16\sigma_T^2 \cos b}{(2\ell + 1)^3}, \quad \ell \rightarrow \infty \quad (14)$$

where σ_T^2 is the variance of the unmasked map

$$\sigma_T^2 = \sum_\ell \frac{2\ell + 1}{4\pi} C_\ell = \left\langle \left(\frac{\Delta T}{T} \right)^2 \right\rangle. \quad (15)$$

On the other hand the white noise spectra are simply multiplied by f_{sky} . Since $\langle \cos \Theta_\ell \rangle \approx \sqrt{\tilde{C}_\ell / (\tilde{C}_\ell + \sigma_N^2)}$, we obtain in the very low signal to noise regime

$$\cos \Theta_\ell \rightarrow \frac{4}{(2\ell + 1)^{3/2}} \left(\frac{\sigma_T}{\sigma_N} \right) \left(\frac{2 - f_{\text{sky}}}{f_{\text{sky}}} \right)^{1/4} \quad (16)$$

Despite the above approximations, these ideas explain the shape of measured Θ_ℓ curves extremely well, and predict asymptotic properties at high ℓ in virtually perfect agreement with simulations and measurements. Note that these considerations do not affect our 5σ decoherence limits, as our null hypothesis of no correlations (corresponding to infinite noise) has no bias.

We used our well calibrated decoherence model to forecast

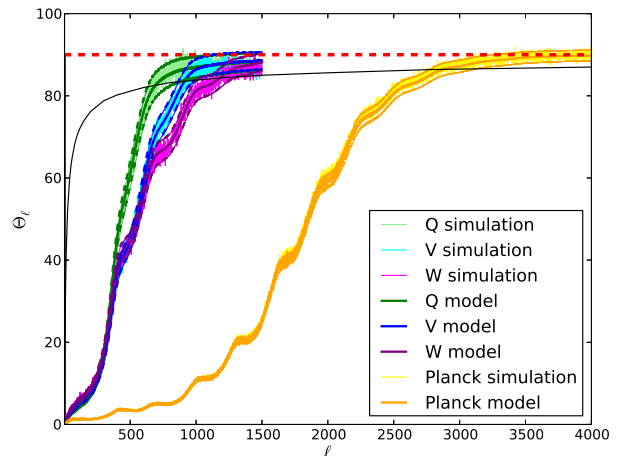


Figure 5. Estimated decoherence properties of a Planck-like simulation ($N_{\text{side}} = 2048$, assuming Smica noise) with a hypothetical perfect CMB experiment with no noise, and our WMAP results for comparison. We show simulated decoherence using single realizations, together with theory and 2σ errors. Black solid line illustrates 5σ significance level for our null hypothesis, while dashed red line shows 90° decoherence level.

GP angles of Planck and a hypothetical perfect CMB experiment without noise (Fig. 5). Decoherence is predicted at $\ell \approx 2900$, beyond which any non-Gaussian information should be dominated by noise.

4 CONCLUSIONS

We quantified the ℓ -by- ℓ coherence of latest WMAP, and Planck CMB maps. We introduced a new set of statistics, Generalized Phases, that are complementary to the (pseudo-)power spectrum, and can be used to characterize the phase-coherence of two CMB maps. We compared GP's of the two maps by simply calculating the angles between the corresponding unit vectors. These angles, while do not contain all non-Gaussian information, concisely summarize the coherence properties of two maps at each ℓ . Using the statistics of random vectors in $(2\ell + 1)$ dimensions, we defined the ℓ of decoherence where the null hypothesis of no correlation between the maps could not be rejected at the 5σ level. We controlled any effect of the masks, typically a problem with statistics based on phases, with careful simulations and analytical models that, albeit based on simplifying assumptions, appear to provide an excellent quantitative framework. To check for systematics, we repeated all our measurements of the Planck Smica map with the NILC maps finding virtually identical results. According to our definition, decoherence from Planck was found above $\ell \approx 700$, $\ell \approx 900$ and $\ell \approx 1100$ for WMAP9 Q, V and W. Our theoretical description is in excellent agreement with the measured coherence angles, with a slight bias for low-intermediate ℓ 's. We also find a small bias of the WMAP pseudo- \tilde{C}_ℓ at $10 \leq \ell \leq 300$ at an average 2.6% level with very high significance. It appears that for high ℓ 's, where our theoretical prediction for the coherence angle is accurate based on a simple Gaussian WMAP noise model, there is no significant bias in the power spectra either. Qualitatively, there is a slight color dependency as well based on Figure 4. From the excess decoherence we can calculate the amount of excess noise it corresponds

to. We found that, with the exception of the Q map in the range of $250 \lesssim \ell \lesssim 500$ the noise corresponding to the excess decoherence is below what is needed to fully explain the bias in the power spectra. Nevertheless, the qualitative behaviour of the noise is similar to the observed one, and it is different than our simulations. In conclusion, there are tantalizing coincidences hinting that the excess decoherence and power spectrum bias are related, but no consistent picture emerged. Note that our simulations do not contain correlated noise, we did not check for any effect of foregrounds or low- ℓ leakage, especially from the dipole, into higher ℓ 's; such investigations are left for future research.

Our analytical and simulation framework can be used to forecast the coherence of Planck with a noise-free experiment (the true CMB). We find that below $\ell \leq 2900$ Planck is coherent with the CMB according to our 5σ criterion, thus non-Gaussian information can be best gleaned from below these ℓ 's.

ACKNOWLEDGMENTS

We acknowledge support from NASA grants NNX12AF83G and NNX10AD53G. In addition, AK acknowledges support from Campus Hungary fellowship program, and OTKA through grant no. 101666.

REFERENCES

- Abramowitz M., Stegun I., 1970, Handbook of mathematical functions. Dover Publications Inc., New York
- Bardeen J. M., Bond J. R., Kaiser N., Szalay A. S., 1986, ApJ, 304, 15
- Bennett C. L., Larson D., Weiland J. L. e. a., 2012, ArXiv e-prints
- Bielewicz P., Eriksen H. K., Banday A. J., Górski K. M., Lilje P. B., 2005, ApJ, 635, 750
- Bond J. R., Efstathiou G., 1987, MNRAS, 226, 655
- Cai T., Fan J., Jiang T., 2013, Technical report of the Department of Statistics, University of Pennsylvania
- Chiang L.-Y., Coles P., 2000, MNRAS, 311, 809
- Chiang L.-Y., Coles P., Naselsky P., 2002, MNRAS, 337, 488
- Chiang L.-Y., Naselsky P. D., 2007, MNRAS, 380, L71
- Chiang L.-Y., Naselsky P. D., Coles P., 2004, ApJ, 602, L1
- Chiang L.-Y., Naselsky P. D., Verkhodanov O. V., Way M. J., 2003, ApJ, 590, L65
- Coles P., Chiang L.-Y., 2000, Nature, 406, 376
- Copi C. J., Huterer D., Schwarz D. J., Starkman G. D., 2006, MNRAS, 367, 79
- Copi C. J., Huterer D., Starkman G. D., 2004, Phys. Rev. D, 70, 043515
- Das S., Souradeep T., 2013, ArXiv e-prints
- Francis C. L., Peacock J. A., 2010, MNRAS, 406, 14
- Frejsel A., Hansen M., Liu H., 2013, JCAP, 6, 5
- Frommert M., Enßlin T. A., 2010, MNRAS, 403, 1739
- Gorski K. M., Hivon E., et al. 2005, ApJ, 622, 759
- Guth A. H., 1981, Phys. Rev. D, 23, 347
- Hansen M., Frejsel A. M., Kim J., Naselsky P., Nesti F., 2011, Phys. Rev. D, 83, 103508
- Hivon E., Górski K. M., Netterfield C. B., Crill B. P., Prunet S., Hansen F., 2002, ApJ, 567, 2
- Jarosik N., Bennett C. L., et al. 2011, ApJS, 192, 14
- Land K., Magueijo J., 2005a, Physical Review Letters, 95, 071301
- Land K., Magueijo J., 2005b, MNRAS, 362, 838

- Land K., Magueijo J., 2007, MNRAS, 378, 153
- Naselsky P. D., Chiang L.-Y., Novikov I. D., Verkhodanov O. V., 2005, International Journal of Modern Physics D, 14, 1273
- Planck Collaboration Ade P. A. R., Aghanim N., Armitage-Caplan et al. 2013a, ArXiv e-prints
- Planck Collaboration Ade P. A. R., Aghanim N., Armitage-Caplan C., et al. 2013b, ArXiv e-prints
- Planck Collaboration Ade P. A. R., Aghanim N., Armitage-Caplan C., et al. 2013c, ArXiv e-prints
- Prunet S., Uzan J.-P., Bernardeau F., Brunier T., 2005, Phys. Rev. D, 71, 083508
- Raeth C., Rossmanith G., Morfill G., Banday A. J., Gorski K. M., 2010, ArXiv e-prints
- Rassat A., Starck J.-L., Dupe F.-X., 2013, ArXiv e-prints
- Stannard A., Coles P., 2005, MNRAS, 364, 929
- Szapudi I., Prunet S., Colombi S., 2001, ApJ, 561, L11

APPENDIX A: THE DISTRIBUTION OF COHERENCE ANGLES FOR NOISY DATA

We derive the form of Eq. (9) next. The probability density for $\cos \Theta_\ell$ is given by

$$p(\cos \Theta) = \int d^n \epsilon_\ell p_G(\epsilon_\ell) \cdot \delta^D \left(\cos \Theta_\ell - \hat{\epsilon}_\ell^{\text{CMB}} \cdot \left(\hat{\epsilon}_\ell^{\text{CMB}} + \hat{\epsilon}_\ell \right) \right), \quad (\text{A1})$$

with δ^D the Dirac delta function and p_G is the probability density describing n Gaussian uncorrelated variables with variance $C_\ell^{\text{noise}}/2$. We can set without loss of generality $\hat{\epsilon}_\ell^{\text{CMB}}$ to be parallel to the first axis, such that

$$\hat{\epsilon}_\ell^{\text{CMB}} \cdot \left(\hat{\epsilon}_\ell^{\text{CMB}} + \hat{\epsilon}_\ell \right) = \frac{C_\ell^{\text{CMB}} + \epsilon_\ell^1}{\sqrt{(C_\ell^{\text{CMB}} + \epsilon_\ell^1)^2 + \sum_{k>1} (\epsilon_\ell^k)^2}}. \quad (\text{A2})$$

Shifting the variable $\epsilon_\ell^1 \rightarrow C_\ell^{\text{CMB}} + \epsilon_\ell^1$ in Eq. (A1) we simplify the integral further. The argument of the integrand depends only of the radial coordinate and of the first polar angle defined by $\epsilon_\ell^1 = r \cos \phi_1$, which must match Θ_ℓ , because of the Dirac delta function. In n -dimensional space we have

$$d^n x = r^{n-1} dr \sin^{n-2} \phi_1 d\phi_1 \cdots. \quad (\text{A3})$$

The Dirac delta function gives the factor $\sin^{n-2} \Theta$ in Eq. (9), and the radial integral the second factor.

APPENDIX B: ESTIMATE OF BIAS SIGNIFICANCE

We define the bias of WMAP with respect to Planck at a given ℓ as

$$b_\ell = \frac{C_\ell^{\text{WMAP}}}{C_\ell^{\text{Planck}}} - 1. \quad (\text{B1})$$

We expect C_ℓ^{WMAP} to coincide on average with C_ℓ^{Planck} , in which case $\langle b_\ell \rangle = 0$. Our aim is to estimate $\langle b_\ell^2 \rangle$. We need to make some simplifying assumptions on the stochasticity of C_ℓ^{WMAP} . We assume that this stochasticity comes from the cross-correlation of two noisy tracers,

$$C_\ell^{\text{WMAP}} = \frac{1}{2\ell + 1} \sum_{m=-\ell}^{\ell} \left(a_{\ell m}^{\text{Planck}} + \epsilon_{1,\ell m} \right) \left(a_{\ell m}^{\text{Planck},*} + \epsilon_{2,\ell m}^* \right), \quad (\text{B2})$$

We assume that the harmonic coefficients $\epsilon_{\ell m}$ of the noise are Gaussian variables with spectrum $\langle \epsilon_{i,\ell m} \epsilon_{j,\ell' m'}^* \rangle = \delta_{\ell\ell'} \delta_{mm'} \delta_{ij} C^{N_i}$, $i, j = 1, 2$, while $a_{\ell m}^{\text{Planck}}$ and C_{ℓ}^{Planck} are simple numbers. Within these assumptions it holds that

$$b_{\ell} = \frac{1}{C_{\ell}^{\text{Planck}} (2\ell + 1)} \sum_{m=-\ell}^{\ell} \left(a_{\ell m}^{\text{Planck}} \epsilon_{2,\ell m}^* + a_{\ell m}^{\text{Planck},*} \epsilon_{1,\ell m} + \epsilon_{1,\ell m} \epsilon_{2,\ell m}^* \right). \quad (\text{B3})$$

Averaging over noise gives no bias, and the variance of b_{ℓ} can be simply evaluated remembering that we treat $a_{\ell m}^{\text{Planck}}$ as simple numbers and that the average of three ϵ 's vanishes. We obtain

$$\langle b_{\ell}^2 \rangle = \frac{1}{2\ell + 1} \left[\left(\frac{C_{\ell}^{N_1} + C_{\ell}^{N_2}}{C_{\ell}^{\text{Planck}}} \right) + \left(\frac{C_{\ell}^{N_1} C_{\ell}^{N_2}}{C_{\ell}^{\text{Planck}}} \right)^2 \right]. \quad (\text{B4})$$

Averaging over multipoles defines the bias $b = (\sum_{\ell} b_{\ell}) / \Delta\ell$. Neglecting correlations, $\langle b_{\ell}^2 \rangle = (\sum_{\ell} \langle b_{\ell}^2 \rangle) / (\Delta\ell)^2$. We set further $C_{\ell}^{N_1} = C_{\ell}^{N_2} = 2C_{\ell}^N$, defining $C_{\ell}^{\text{Planck}} / C_{\ell}^N$ as the signal to noise SN_{ℓ} of the map. Thus we obtain our final formula

$$\langle b^2 \rangle = \frac{4}{(\Delta\ell)^2} \sum_{\ell_{\min}}^{\ell_{\max}} \left(\frac{1 + SN_{\ell}}{(2\ell + 1) (SN_{\ell})^2} \right), \quad (\text{B5})$$

with $\Delta\ell = \ell_{\max} - \ell_{\min} + 1$, with which we estimated the significance of the bias.

For a roughly constant signal to noise a simple estimate of $\sigma_b = \sqrt{\langle b^2 \rangle}$ is

$$\sigma_b \approx \frac{2\sqrt{1 + SN}}{\Delta\ell SN} \sqrt{\ln \left(\frac{\ell_{\max}}{\ell_{\min}} \right)}. \quad (\text{B6})$$

Using the above formula and neglecting correlations between C_{ℓ} 's, we estimate the significance of the bias in the Q,V,W colors to be 33σ , 30σ and 26σ , respectively. While taking into account the true covariance matrix, potentially impacted by correlated noise and mask, could lower these significances, it is safe to state that the bias below $\ell \lesssim 300$ is overwhelmingly significant. At the same time, if ℓ 's up to 1100 - the maximum given by ℓ_{\max} of Q1,Q2 beam transfer functions - are taken into account, we find 1.6σ , 0.7σ , and 1.2σ , i.e. no significant bias is detected over the full range of the power spectrum. Note, however, that this is mainly due to the noise dominating at high ℓ and the uniform weighting of our estimator, that is suboptimal for the bias once the noise is increasing due to the tail of the beam correction.

APPENDIX C: COHERENCE ANGLE ASYMPTOTICS WITH AZYMUTHALLY SYMMETRIC MASK

We derive the asymptotic behavior of the coherence angle in the presence of an azimuthally symmetric mask (band). Our starting point is the exact formula relating the spectrum of the original map to that of the masked map (Hivon et al. 2002)

$$C_{\ell}^{\text{masked}} = \sum_{\ell_2 \ell_3} = \frac{2\ell_2 + 1}{4\pi} C_{\ell_2} |W_{\ell_3 0}|^2 \begin{pmatrix} \ell & \ell_2 & \ell_3 \\ 0 & 0 & 0 \end{pmatrix}^2. \quad (\text{C1})$$

In this equation $W_{\ell 0}$ are the harmonic coefficient of the azimuthally symmetric mask function. We are interested in the regime where $\ell \rightarrow \infty$. In this case, it is possible to rewrite the above equation as follows,

$$C_{\ell}^{\text{masked}} \xrightarrow{\ell \rightarrow \infty} \frac{1}{2\ell + 1} \sum_{\ell_2} \frac{2\ell_2 + 1}{4\pi} C_{\ell_2} \langle |W_{\ell_2 0}|^2 \rangle_{\ell - \ell_2, \ell + \ell_2}, \quad (\text{C2})$$

where the last term is the average of $|W_{\ell_2 0}|^2$ with a roughly flat weight function centered on ℓ with width ℓ_2 . The exact weight function can be obtained from the asymptotics of the Wigner $3j$ symbols (Hivon et al. 2002, e.g.) but they turn out irrelevant for our purpose. For a band mask centered on the equator with angle b , and thus $f_{\text{sky}} = 1 - \sin b$, we have

$$W_{\ell 0} = \sqrt{\frac{4\pi}{2\ell + 1}} (P_{\ell-1}(\sin b) - P_{\ell+1}(\sin b)), \quad \ell \text{ even}. \quad (\text{C3})$$

where $P_{\ell}(x)$ are the Legendre polynomials. The coefficients for ℓ odd vanish due to the symmetry with respect to the equator. The polynomials have the asymptotic behavior

$$P_{\ell}(\cos \theta) \rightarrow \frac{2 \cos \left((\ell + 1/2)\theta - \frac{\pi}{4} \right)}{\sqrt{\pi(2\ell + 1) \sin \theta}}, \quad (\text{C4})$$

at high ℓ . Using this formula and the addition formula for sines and cosines, one has after some algebra

$$W_{\ell 0}^2 \rightarrow \frac{64}{(2\ell + 1)^2} \sin \theta \sin^2 \left((\ell + 1/2)\theta - \frac{\pi}{4} \right), \quad \ell \text{ even}, \quad (\text{C5})$$

with $\theta = \pi/2 - b$ and $\sin \theta = \cos b$. We need the mean value of (C5) with respect to a smooth function centered on ℓ with size $2\ell_2$, small with respect to ℓ . We can replace the \sin^2 in (C5) by a factor $1/2$, as the average would be the same if \sin^2 was in fact a \cos^2 . Another factor $1/2$ comes from the fact that only even ℓ are non-zero.

$$\begin{aligned} C_{\ell}^{\text{masked}} &\xrightarrow{\ell \rightarrow \infty} \frac{1}{2\ell + 1} \sum_{\ell_2} \frac{2\ell_2 + 1}{4\pi} C_{\ell_2} \langle |W_{\ell_2 0}|^2 \rangle_{\ell - \ell_2, \ell + \ell_2} \\ &\sim \frac{16 \cos b}{2\ell + 1} \sum_{\ell_2} \frac{(2\ell_2 + 1)}{4\pi} C_{\ell_2} \left\langle \frac{1}{(2\ell + 1)^2} \right\rangle_{\ell - \ell_2, \ell + \ell_2} \end{aligned} \quad (\text{C6})$$

If C_{ℓ_2} only for ℓ_2 much smaller than ℓ , then the mean value becomes independent of ℓ_2 . All in all, we obtain

$$C_{\ell}^{\text{masked}} \rightarrow \frac{16 \cos b}{(2\ell + 1)^3} \left(\sum_{\ell_2} \frac{(2\ell_2 + 1)}{4\pi} C_{\ell_2} \right) \quad (\text{C7})$$

The last term is the variance of the map. This formula is valid both for small or large f_{sky} .